Light-based feedback for controlling intracellular signaling dynamics

Jared E Toettcher, Delquin Gong, Wendell A Lim & Orion D Weiner

|	
Supplementary Figure 1	Optimizing conditions for quantitative imaging of the Phy-PIF module
Supplementary Figure 2	Measuring the Phy-PIF module's dose response across a population of cells
Supplementary Figure 3	Fitting a biochemical model of the Phy-PIF module to dose response data
Supplementary Figure 4	The frequency responses of PIF recruitment and PI3K activity
Supplementary Figure 5	Modeling the proportional-integral (PI) feedback controller
Supplementary Figure 6	Feedback control reduces cell-to-cell variability in PIF recruitment
Supplementary Figure 7	Feedback control reduces cell-to-cell variability in PIF recruitment
Supplementary Figure 8	Light-gated PI3K lipid product generation is spatially restricted, fast-responding, and induces cell protrusion
Supplementary Figure 9	Quantitative input-output characterization of light-gated PI3K signaling
Supplementary Note 1	Detailed description of feedback controller; additional experimental and computational methods

Note: Supplementary Software 1 is available on the Nature Methods website.

Supplementary Figure 1
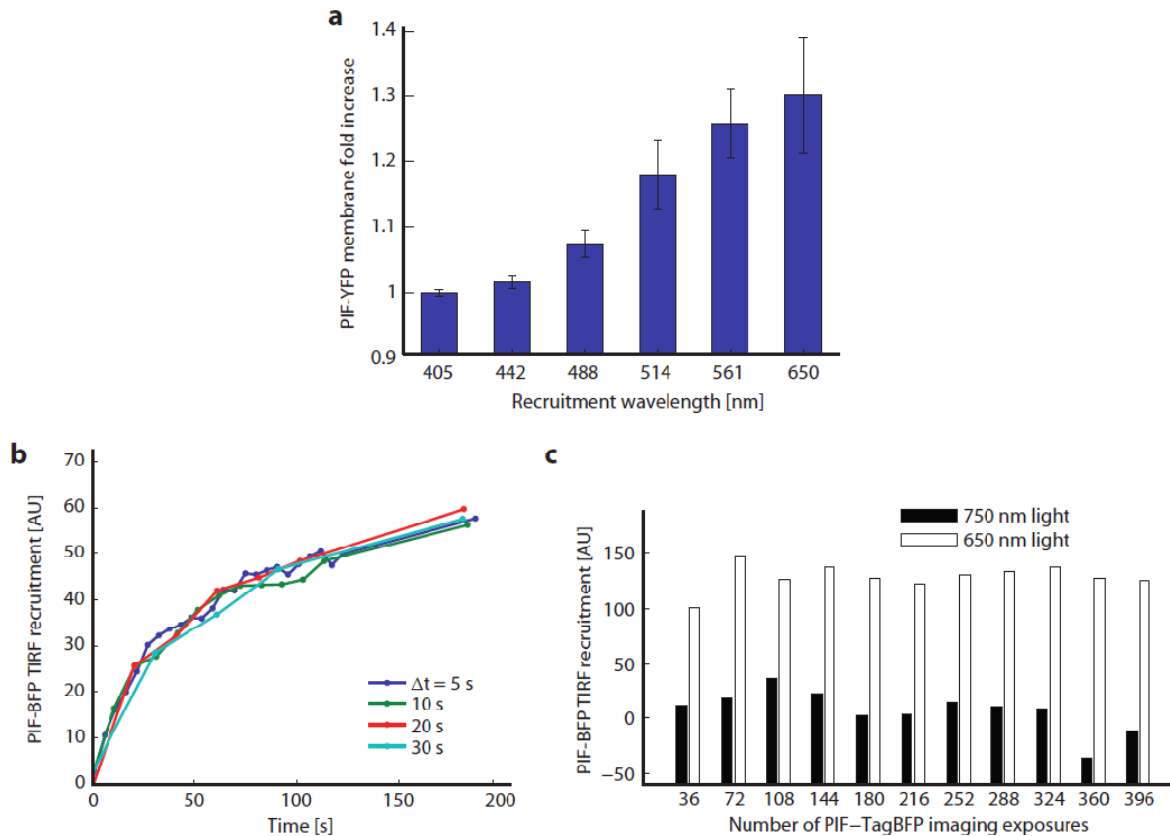
Optimizing conditions for quantitative imaging of the Phy–PIF module. (**a**) NIH-3T3 cells expressing Phy-mCherry-CAAX and PIF-YFP were exposed to 30 s of constant laser illumination at different wavelengths, from 405 nm to 561 nm. As a positive control, 650 nm light was applied using the 650 nm LED normally used to activate Phy-PIF association. Each bar shows the mean + S.E.M. of 5 cells. (**b**) Imaging does not affect the maximum level or kinetics of PIF-BFP recruitment. Data shown reflects measurements from an NIH-3T3 cell expressing Phy-mCherry-CAAX and PIF-BFP. Constant 650 nm light was applied starting at t = 0, and recruitment was measured by imaging at 405nm at a frequency of 5, 10, 20 or 30 s for a total of 200 s. The initial unrecruited intensity was subtracted from all intensity values. (**c**) At low imaging intensity, photobleaching is negligible. Data shown reflects measurements from a cell expressing the same constructs as in **b**, exposed to 396 BFP imaging exposures over 4 hours. Every 36 images, cells were exposed to 30 s of 650 nm or 750 nm light to determine maximum and minimum recruitment. The initial unrecruited intensity was subtracted from all intensity values.

Supplementary Figure 2
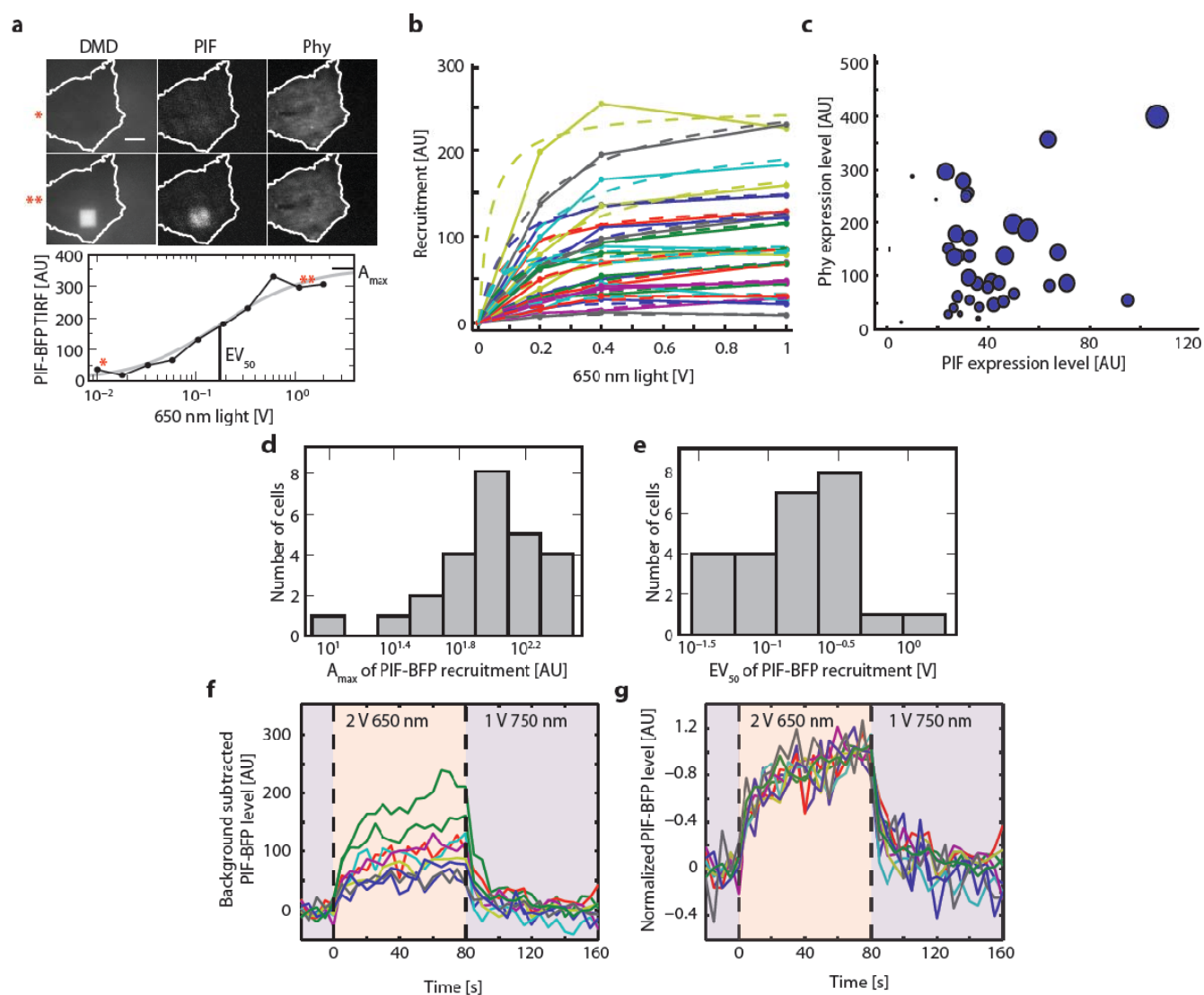
Measuring the Phy–PIF module's dose response across a population of cells. (**a**) Upper panels: single-cell TIRF images of optogenetic recruitment taken at low (*) and high (**) activating light levels. Scale bar: 10 µm. Lower panel: the dose response of membrane recruitment with light, showing the half-maximal voltage (EV_{50}) and maximum recruitment A_{max}. DMD: digital mirror device. (**b**) Dose response curves across a population of cells exhibiting recruitment, with fits to a simple binding saturation model. (**c**) Maximal PIF recruitment (represented by size of circle) plotted as a function of Phy-mCherry-CAAX and PIF-BFP expression across a population of cells. (**d,e**) Variability in A_{max} (**d**) and EV_{50} (**e**) between cells in **b**. (**f,g**) Transient response for nine cells expressing PIF-BFP and Phy-mCherry-CAAX, stimulated with 2 V 650 nm light at t = 0 s, and 1 V 750 nm light at t = 80 s. Background subtracted (**f**) and normalized (**g**) BFP TIRF signals are shown.

Supplementary Figure 3
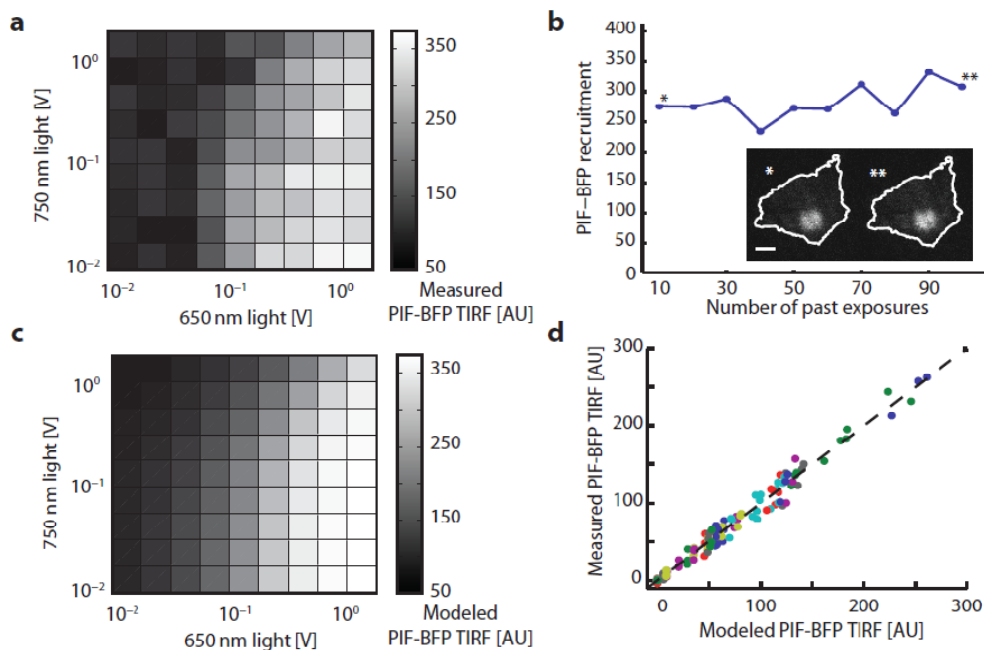
Fitting a biochemical model of the Phy–PIF module to dose response data. (**a**) Measured PIF-BFP membrane recruitment at different 650 and 750 nm light intensities in a single cell. (**b**) Control recruitment intensity in response to 1 V 650 nm and 0.1 V 750 nm light, acquired every 10 images for the cell used to establish 650/750 dose response curve in **a**. Intensity does not decrease systematically over time, indicating that photobleaching is negligible. Inset shows images of the cell at the first and last images with the same intensity scaling. Scale bar: 10 µm. (**c,d**) A mathematical model of the Phy–PIF interaction fits population (**c**) and single-cell (**d**) dose response data. Data points in **d** are colored to represent the corresponding trajectories in **Supplementary Fig. 2b**.

Supplementary Figure 4
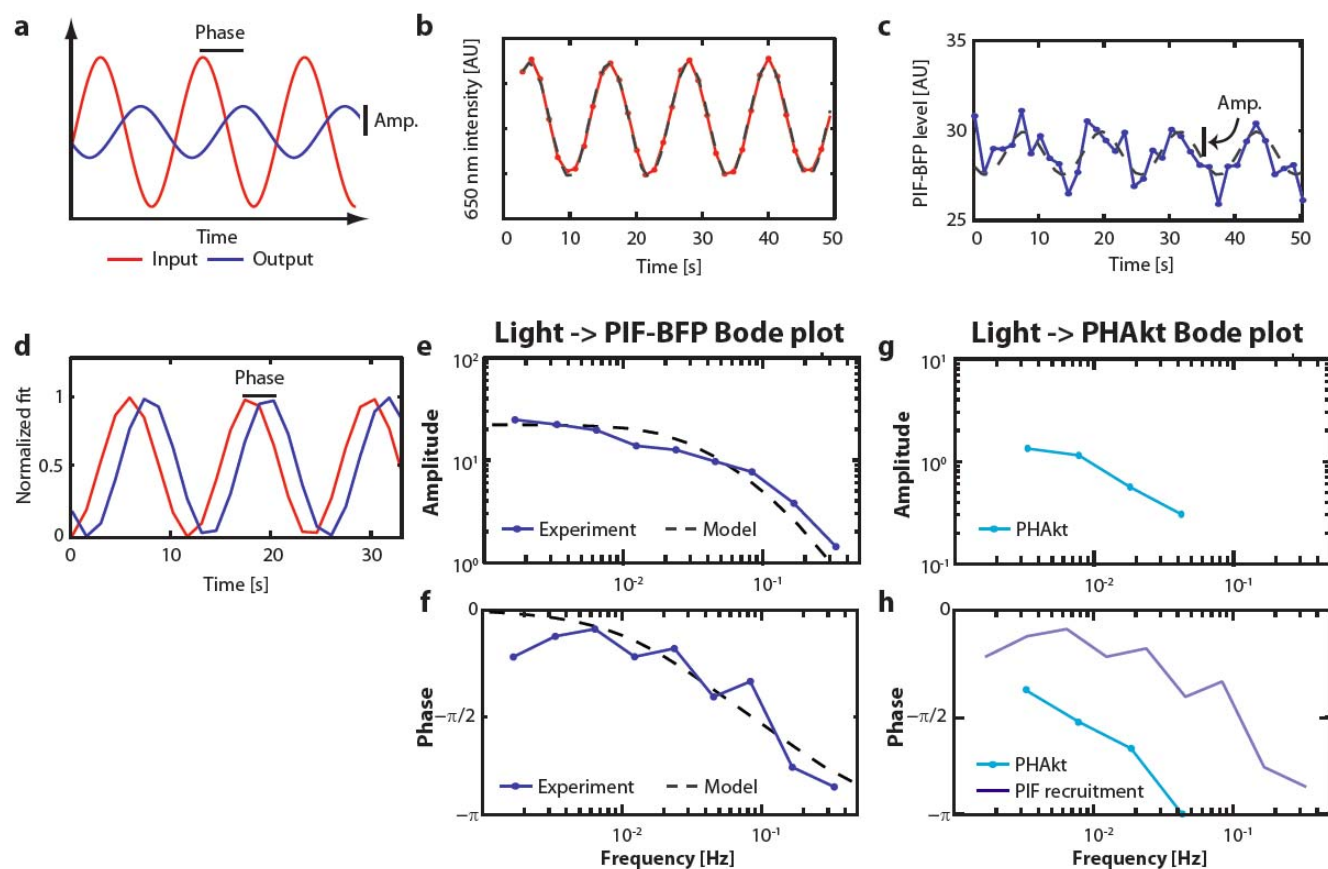
The frequency responses of PIF recruitment and PI3K activity. (**a**) Schematic of a linear system's response (blue) to a sinusoidal input (red), incorporating both a change in amplitude and phase. (**b,c**) Typical frequency response data from PIF-BFP cells stimulated with a 0.083 Hz input. Raw data (red and blue curves) and sinusoidal fits (dashed black curves) shown for (**b**) 650 nm input light intensity and (**c**) PIF-BFP TIRF intensity. (**d**) The overlay of sinusoidal fits from (**b,c**), showing the measured phase shift between input and output. (**e,f**) Bode plots of the PIF-BFP frequency response (blue curves), calculated by applying the methodology of (**a-d**) at multiple frequencies. Also shown is the frequency response generated from our model stimulated by sinusoidal light inputs (dotted black curves). (**g,h**) Bode plots of light-gated PI3K activity showing PHAkt-Cerulean membrane translocation amplitude and phase. In panel (**h**), the dark blue curve from (**f**) is reproduced for comparison.

Supplementary Figure 5
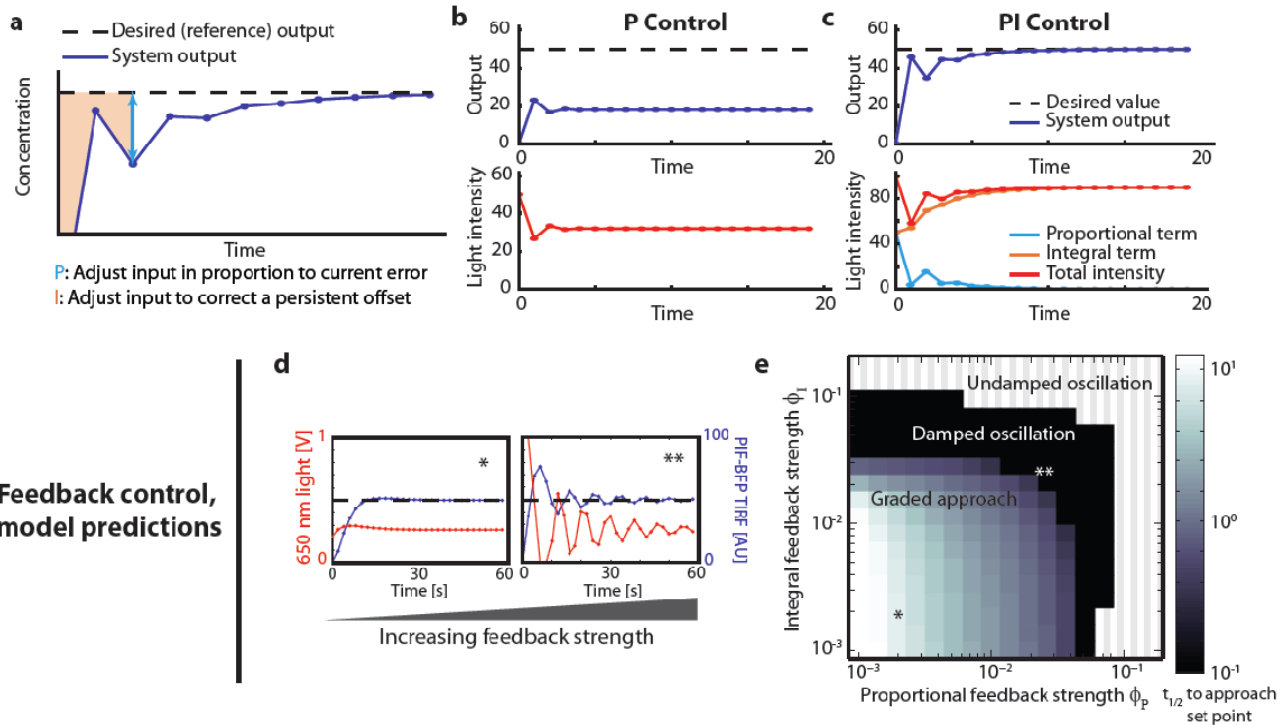
Modeling the proportional-integral (PI) feedback controller. (**a**) Control simulation showing the current error (cyan) and the integral error (orange shaded area). (**b,c**) Control simulation using proportional feedback alone (**b**) or in combination with integral feedback (**c**). Upper plots show system output levels; lower plots show corresponding light levels. (**d**) PI control applied to a model of PIF-BFP recruitment at low (left panel) and high (right panel) feedback strengths. (**e**) Heatmap showing the time required for control as the proportional (ϕ_P) and integral (ϕ_I) feedback strengths vary. Hatched region indicates undamped oscillation around the reference value.

Supplementary Figure 6
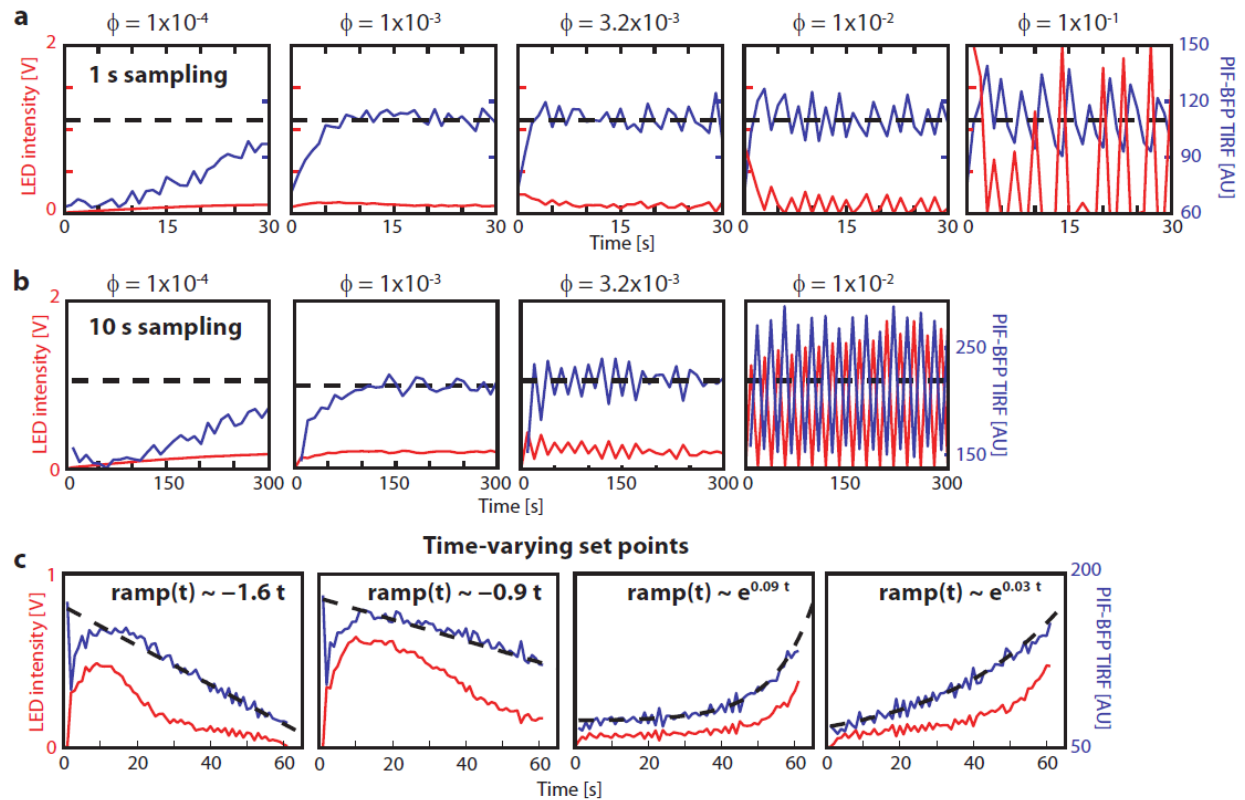
Characterizing the robustness of the (PI) feedback controller. (**a**) Each panel shows data collected from the same single cell, where the strength of proportional and integral feedback are co-varied (the value of each is represented above the panel as ϕ). Weak feedback leads to a slow response; strong feedback leads to undamped oscillation. (**a**) Each panel shows data from the same single cell. Feedback strengths are varied as in (**a**), but the time between samples is 10 s. Strong oscillation occurs at lower feedback strength, indicating that sparse sampling time destabilizes the controller. (**c**) Experimental data showing the ability of the controller to direct linear and exponential ramps with varying steepness of PIF recruitment to the plasma membrane. For each curve in **c**, $\phi = 2.5 \times 10^{-3}$.

Supplementary Figure 7
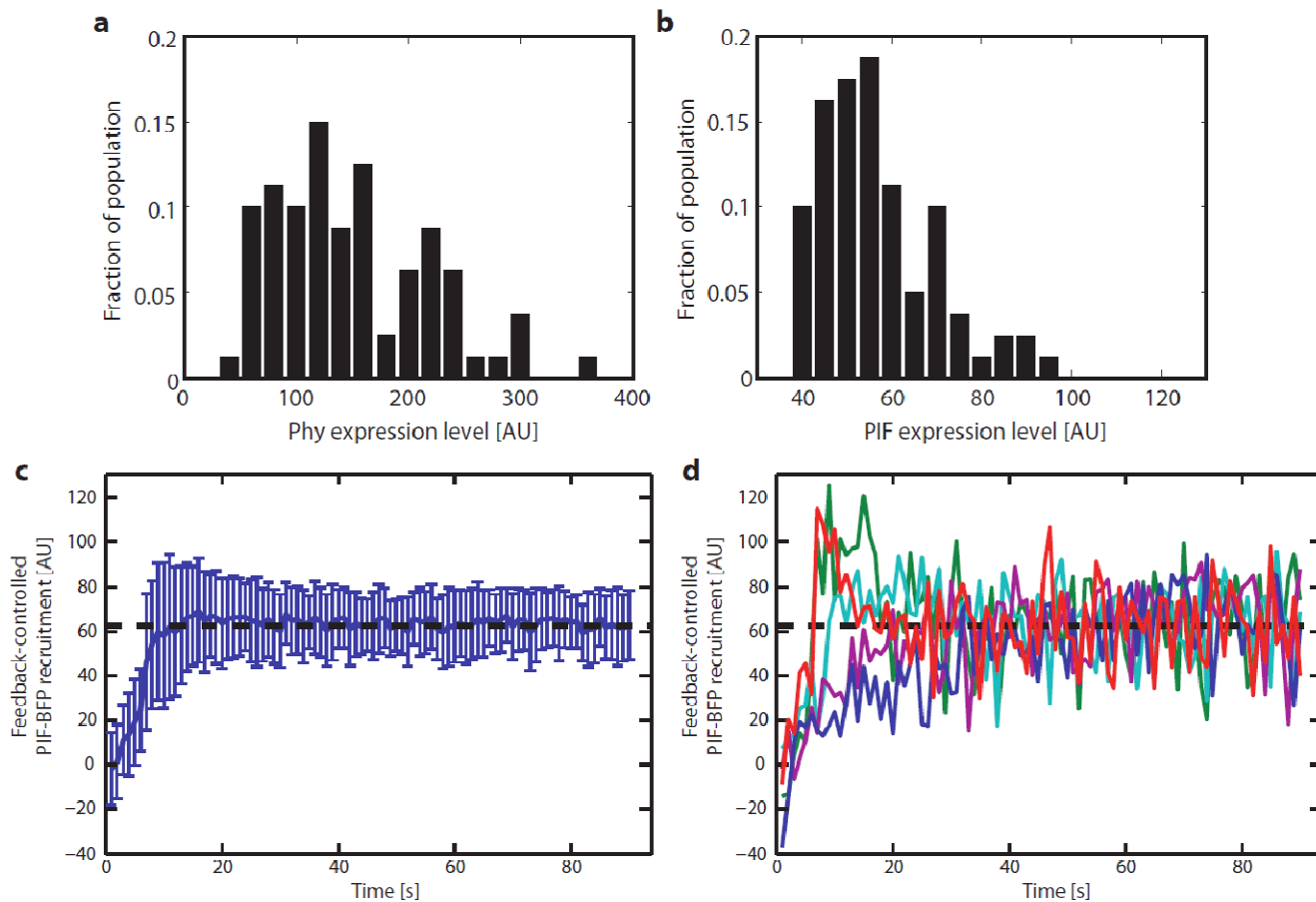
Feedback control reduces cell-to-cell variability in PIF recruitment. (**a,b**) Phy-mCherry-CAAX (**a**) and PIF-BFP (**b**) expression levels measured by TIRF microscopy from the same cells used in **Fig. 2** under 750 nm light (*i.e.* lacking recruitment). Both Phy and PIF levels vary widely across the population. (**c**) The mean PIF recruitment from 60 randomly selected cells (solid blue line) and the standard deviation of PIF recruitment (error bars) are shown at each timepoint during 90 s of feedback control to a single set point (dashed black line). (**d**) Five representative single-cell traces from the cell population in (**c**) are shown in gray; the set point is indicated by the dashed black line.

Supplementary Figure 8
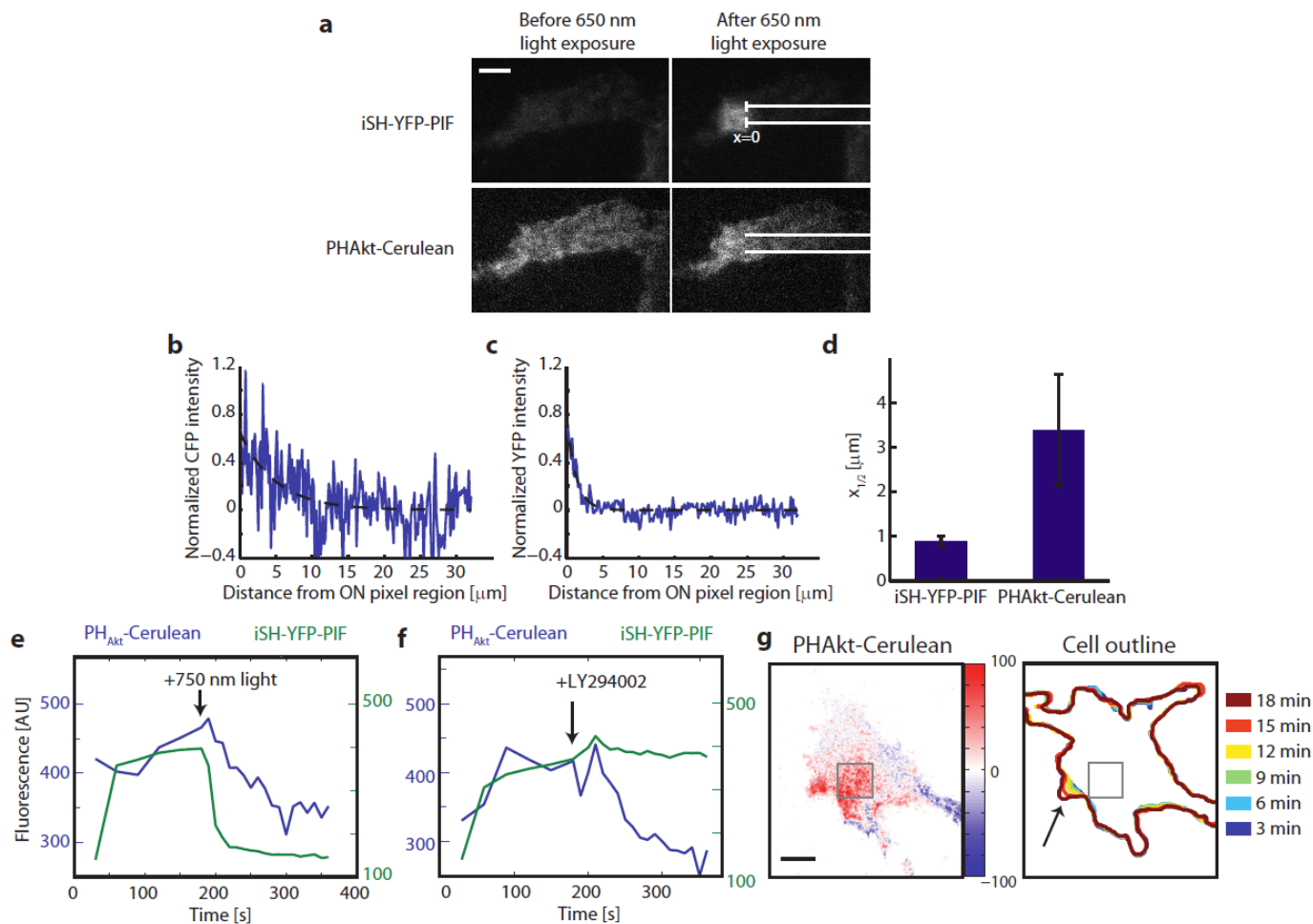
Light-gated PI3K lipid product generation is spatially restricted, fast-responding, and induces cell protrusion. (**a**) A representative NIH-3T3 cell expressing Phy-mCherry-CAAX, iSH-YFP-PIF, and PHAkt-Cerulean was locally stimulated with 650 nm light, leading to a local increase in PHAkt-Cerulean signal (gray lines show the region analyzed for panels **b,c**). Scale bar: 10 μm. (**b,c**) Line profiles quantifying the change in PHAkt-Cerulean (**b**) and PIF-YFP (**c**) plasma membrane recruitment after spatially restricted recruitment show a decrease with distance from the edge of the ON pixel region (indicated as x = 0). Exponential decay fits are shown with dotted lines. (**d**) The distance for half of the decay to occur, $x_{1/2}$, was quantified from (b-c). Best-fit +/- 95% confidence limits shown. (**e,f**) 750nm light causes iSH-YFP PIF to rapidly dissociate from the plasma membrane (**e**), and results in a rate of PI3K lipid product disappearance ($t_{1/2}$ = 48 s), which is comparable to that after PI3K inhibition by 100 μM LY294002 (**f**; $t_{1/2}$ = 65s). (**g**) Cell protrusion is observed near the site of PI3K recruitment. The left panel shows relative increase in PHAkt-Cerulean after 18 minutes of recruitment; the right panel shows the cell outline measured every 3 minutes during PI3K recruitment.

Supplementary Figure 9
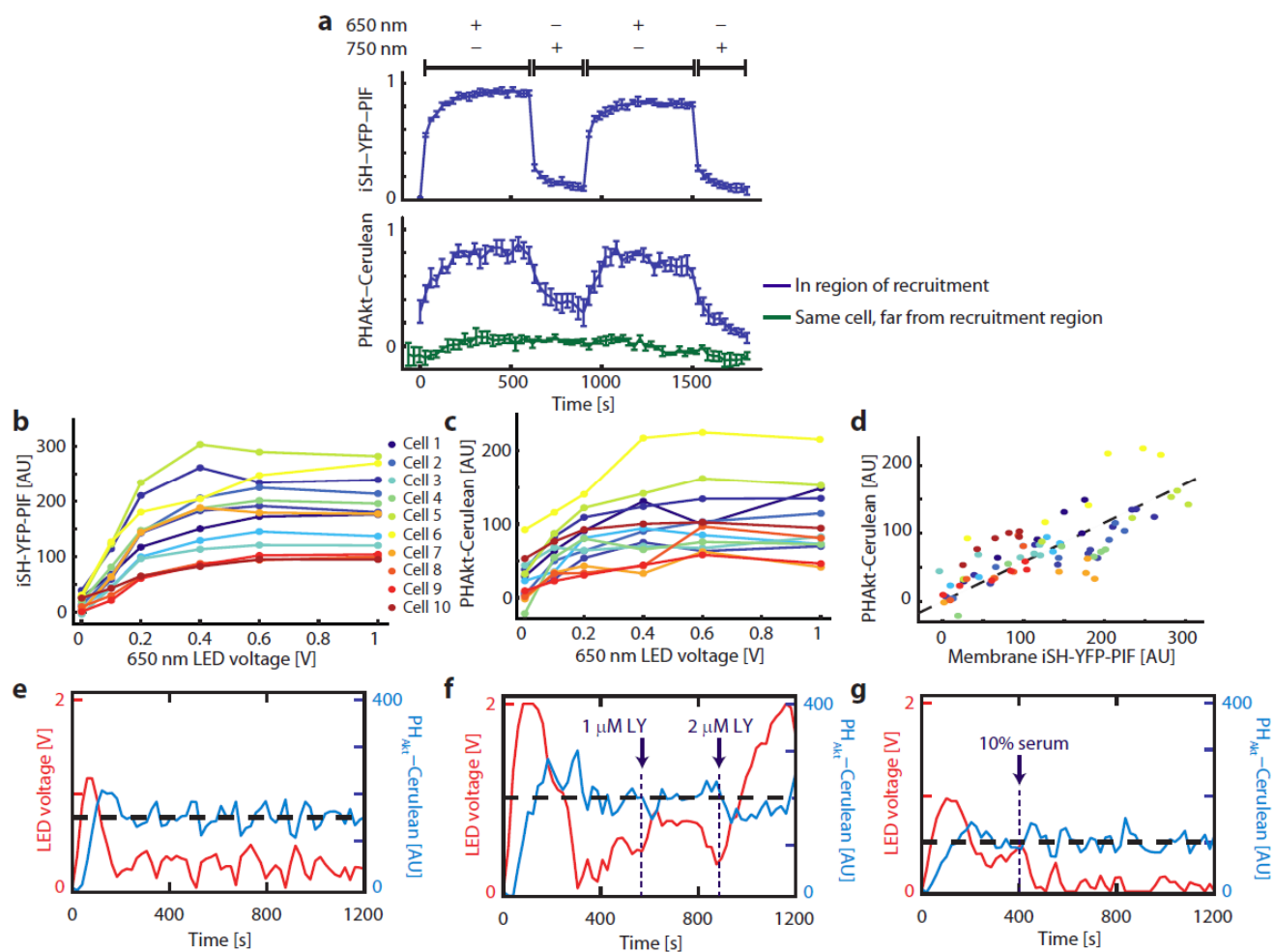
Quantitative input-output characterization of light-gated PI3K signaling. (**a**) PI3K lipid product generation measured by membrane PHAkt-Cerulean translocation to the illuminated region (lower plot, blue curve) or another region in the same cell (green curve) in response to repeated rounds of iSH-YFP-PIF recruitment (upper plot). Plots show mean + standard error from five cells. For normalized fluorescence, we subtract background fluorescence in 750 nm exposed (unrecruited) cells and divide by the maximum recruitment. (**b,c**) iSH-YFP-PIF (**b**) and PHAkt-Cerulean (**c**) recruitment as a function of 650 nm voltage in 10 cells. Cells were allowed to equilibrate for light for 3 minutes before quantifying recruitment. (**d**) Recruited iSH-YFP-PIF levels are linearly related to the level of PHAkt-Cerulean recruitment. Each data point from **b,c** is represented, and points are colored by cell number as in **b,c**. (**e-g**) Sequential experiments in a single cell show feedback control of PHAkt-Cerulean can clamp PIP$_3$ against perturbation. Constant PIP$_3$ levels are maintained in control cells (**e**), following addition of PI3K inhibitor LY294002 (**f**), or following addition of 10% serum (**g**; serum activates endogenous PI3K). 650 nm LED voltage (red), normalized PHAkt-Cerulean recruitment (blue) and the feedback controlled value (dotted black) are shown.

Supplementary Note

Table of Contents

Quantifying Phy–PIF dose response curves: modeling and experiments

Experimental design

    We first set out to inform a mathematical model that could recapitulate both how 650 nm and 750 nm light affect recruitment and how cell-to-cell variability in optogenetic component expression changes this response. As discussed below, this model proved to be a valuable tool for prototyping feedback controller designs. To inform this model, we experimentally measured

1

dose response curves of PIF-BFP membrane recruitment (see **Supplementary Fig. 2a** for a typical example) across a population of cells and at multiple 750 nm light levels in a single cell.

We first measured dose response curves from a population of 35 randomly selected cells (**Supplementary Fig. 2b**, solid lines). Each cell was stimulated with 0, 0.2, 0.4, and 1 V 650 nm light in the presence of 0.1 V 750 nm light, after which measurements from the next cell were conducted. Images of recruitment were acquired after 120 seconds of equilibration to each light dose. We compared the recruitment observed at 1V 650 nm light to both the Phy and PIF expression levels (measured by mCherry and BFP imaging, respectively) and found that increased level of expression of both components correlated with higher potential for recruitment (**Supplementary Fig. 2c**). By fitting the dose response curves to a simple binding saturation model (**Supplementary Fig. 2b**, dotted lines), we found that individual cells can vary tenfold in both their maximum achievable recruitment (A_{max}; **Supplementary Fig. 2d**) as well as the 650 nm voltage driving half-maximal activation (EV_{50}; **Supplementary Fig. 2e**).

To more completely characterize the response to varying levels of 650 and 750 nm light, we measured the full matrix of recruitment in response to ten logarithmically-spaced intensities of 650 and 750 nm light (**Supplementary Fig. 3a**). Images of recruitment were acquired after 120 seconds of equilibration to each light dose. To avoid systematic errors caused by changes to the cell's responsivity over time, we measured these light conditions in a random order. Moreover, after every 10 conditions, we performed a measurement at a control dose (1 V 650, 0.1 V 750) to ensure that the maximum recruitment was unchanged over time (**Supplementary Fig. 3b**).

Fitting data with a binding saturation model

To gain insight into the variability of PIF dose response curves between individual cells, we fit each cell's dose response data to a binding saturation model. We found that a Hill coefficient

2

of 1 was able to fit each cell's response well; thus, as expected, the Phy–PIF interaction is not cooperative. For each cell, we fit two parameters: the light level at which binding was half-maximal (EV_{50}) and the maximum level of PIF binding (A_{max}). Binding saturation curve fits were performed using the MATLAB Curve Fitting Toolbox's `fit` function. 7/35 cells exhibited very low levels of recruitment at all light doses. Because their analysis resulted in poor estimates of A_{max} and EV_{50}; they were excluded from **Supplementary Fig. 2d,e**.

Fitting a biochemical model of the Phy–PIF module

We next asked whether a single biochemical model of the Phy–PIF module is consistent with all of our measured steady state data. To this end, we derived a simple mass-action biochemical model of the Phy–PIF interaction. This model incorporates two processes: interconversion of Phy between two conformations (f and f^*), and the binding of PIF (p) to one of the two conformations (forming the complex c):

$$\frac{df^*}{dt} = 0 = k_{f,650} u_{650}\left(f_T - f^*\right) - k_{r,750} u_{750} f^* - k_{r,basal} f^*$$

$$\frac{dc}{dt} = 0 = k_a\left(p_T - c\right)f^* - k_d c$$

Our model includes 5 biochemical parameters: the light-dependent photoisomerization rates ($k_{f,650}$ and $k_{r,750}$), light-independent rate of switching to the off state ($k_{r,basal}$), and the association and dissociation rates for PIF binding (k_a and k_d). We assumed that the rates of photoisomerization were linearly proportional to the 650 nm and 750 nm light voltage applied (u_{650} and u_{750}). Note that this model can be either solved for the complex concentration c at steady state (by setting time derivatives to zero as indicated), or simulated over time to generate a transient response to changes in light levels.

3

To solve for the steady state level of bound Phy–PIF, the total Phy (f_T) and PIF (p_T) protein concentrations must also be specified. We were able to observe one of these quantities experimentally, using TIRF measurements of Phy-mCherry-CAAX membrane concentration from each cell. Because of the challenge in measuring the ratio of total Phy and PIF in each cell (which requires measurement of each cell's surface area to volume ratio and cytoplasmic PIF levels), we left PIF concentration as a free parameter for each cell's fit, and simultaneously fit the five rate constants and PIF concentrations to the dose response data described above. The simultaneous fitting of our biochemical model to all data was performed using the MATLAB Optimization Toolbox's `fmincon` function.

It should be noted that all of the data provided to our fitting procedure was collected at steady state and therefore cannot constrain the overall timescale at which equilibrium is approached. By scaling the value of all five parameters together, this timescale could be varied while leaving all steady state levels unchanged. We used data indicating the rate of approach to equilibrium (**Supplementary Fig. 1b; Supplementary Fig. 2f-g** shows switching times for a population of cells) to set this timescale in the model, constraining this last degree of freedom. The resulting parameter values are shown in **Supplementary Table 1**, and the quality of model fits are shown in **Supplementary Fig. 3c** (multiple 750 nm light levels) and **Supplementary Fig. 3d** (multiple cells).

Parameter name (units)	$k_{f,650}$ $(s^{-1}V^{-1})$	$k_{r,750}$ $(s^{-1}V^{-1})$	$k_{r,basal}$ (s^{-1})	k_a $(s^{-1}[Phy]^{-1})$	k_d (s^{-1})
Parameter value	0.399	0.585	0.1727	5.196×10^{-4}	0.419

Supplementary Table 1. Best-fit model parameters to the steady state data at various 650 and 750 nm light levels, and constrained by transient data.

The frequency response of the PIF-BFP module: measurements and modeling

Frequency domain analysis represents a powerful tool for characterizing a system's response to time-varying inputs. For such analyses, a system is driven with an oscillating input at various frequencies and both the output's amplitude and its shift in phase from the input are measured (**Supplementary Fig. 4a**)[1]. The frequency response can concisely represent the dynamic behavior for signaling pathways – including the number of biochemical reactions modulating output and the timescale on which they act –as long as the pathway behaves approximately as a linear system. Even for nonlinear systems, this criterion is often at least satisfied for small oscillation amplitudes. In this section, we measure the frequency response of the Phy–PIF membrane binding module, and compare it to computational results from the model described above.

We applied sinusoidal 650 nm light levels to stimulate individual cells expressing PIF-BFP and Phy-mCherry-CAAX. To ensure frequency measurements were made at steady state, cells were pre-equilibrated to 2 minutes of sinusoidal inputs at each frequency. After pre-equilibration, PIF-BFP and 650 nm input light levels were measured by TIRF microscopy at nine points per period over four periods. Typical traces of the measured input sinusoid and the oscillating PIF-BFP levels it induces are shown in **Supplementary Fig. 4b,c**. We fit both input and output measurements to a sinusoidal curve, and computed the amplitudes (**Supplementary Fig. 4c**) and phase shifts (**Supplementary Fig. 4d**) associated with each oscillating signal.

Applying this analysis at multiple frequencies allowed us to measure the Phy–PIF module's amplitude and phase Bode plots (**Supplementary Fig. 4e,f**). We next set out to interpret the Bode plots in the context of linear systems theory. The phase Bode plot demonstrates a total phase shift of approximately $-\pi$ radians, corresponding to a transfer function with two poles.

5

Biologically, this result would be expected from a biochemical system with two sequential reactions between input and output (because in each reaction the time derivative of output is proportional to inputs, and each derivative contributes a total phase shift of $-\pi/2$ radians). We find that this phase shift occurs at a characteristic frequency of approximately 0.1 Hz, corresponding to our intuition that Phy–PIF binding occurs in about 10 s.

As suggested by the frequency response measurements, our mathematical model implements two serial reactions: light first induces a change in conformation of Phy, and Phy in the Pfr state subsequently binds PIF. To quantitatively compare model and experiment, we measured the frequency response from the model described in the prior section. We simulated the model under a sinusoidal 650 nm light input and applied the same analysis routine to measure its frequency response, finding a close match with the measured data (**Supplementary Fig. 4e,f**, dashed black lines).

Feedback control modeling and experiments

Controller design

This section describes the feedback control strategy we used to manipulate membrane recruitment of various PIF-tagged fluorescent fusion proteins, a core technology of this work (**Fig. 1b**). For setting a feedback-controlled constant output level, the controller is provided with a quantity termed the error $E[t_i]$, defined as the difference between the desired constant level (input; $y_{reference}$) and the current amount of binding (output; $y_{exp\,eriment}[t_i]$):

$$E[t_i] = y_{reference} - y_{exp\,eriment}[t_i].$$

For experiments where the controller was used to drive time-varying activity levels, the experimental output must track a continually moving target (defined as the time-varying

6

reference function $y_{reference}[t_i]$). In this case, tracking is improved when the controller is used in a predictive mode, so that the error is defined as the difference between the current output $y_{experiment}[t_i]$ and the *next* timepoint's desired value $y_{reference}[t_i]$:

$$E_i = y_{reference}[t_{i+1}] - y_{experiment}[t_i].$$

In both cases, this process is repeated at each sampled measurement time t_i, and the error is used by the controller to compute a new value for the light intensity with which to drive the biological system.

For all feedback control experiments in this study, we used a controller implementing both proportional and integral (PI) control terms (**Supplementary Fig. 5a**). PI controllers are among the simplest and most widely used for a variety of applications, and are a special case of the more general class of proportional-integral-derivative (PID) controllers. A PI controller adjusts inputs in proportion both to the current error (the proportional term, shown in cyan, **Supplementary Fig. 5a,c**) and the sum of past errors (integral term; orange, **Supplementary Fig. 5a,c**). This strategy offers a marked improvement over using proportional control alone, which can never drive the system output to exactly match the desired value (compare **Supplementary Fig. 5b,c**). We favored PI over PID control because the derivative control term can be quite sensitive to noise, which we found to be significant in measurements of membrane fluorescence. Our PI feedback control strategy has three tunable parameters: the strength of integral feedback ϕ_I, the strength of proportional feedback ϕ_P, and the sampling time between measurements of system output t_s. The PI feedback controller was implemented at the nth time step using the equation

7

$$u_{650}[t_n] = \phi_I \sum_{i=1}^{n} E[t_i] - \phi_P E_n \, .$$

Controlling the fitted Phy–PIF model

We prototyped the PI feedback controller using our fitted biochemical model of the Phy–PIF interaction. We simulated Phy–PIF dynamics from our differential equation model fitted to single-cell dose response data using the `ode15s` solver in MATLAB (The Mathworks). After simulating the ODE system under a constant light input for the sampling time t_s, our feedback controller computed the error and adjusted the model's light input appropriately. The value of t_s was chosen to mimic the measurement timescale accessible in our experimental system, and was set to either 1 s or 2 s for all simulations. In each simulation, feedback control was run for at least 100 output samples. To measure the rate of approach to the reference value (**Supplementary Fig. 5e**), we fit the error E to an exponential decay function using the MATLAB curve fitting toolbox, and computed the half-life of this decay.

Simulations at varying feedback strengths demonstrated that the PI controller undergoes undamped oscillations at high values of either the proportional or integral feedback terms (**Supplementary Fig. 5d,e**). It is known that applying strong integral feedback to a system can be destabilizing, but oscillation at high levels of proportional feedback is less typical. It arises in our system because measurements are not performed continuously, but are sampled at discrete times t_s. Because the amount of PIF membrane binding can change significantly between successive output measurements, the system can over- and undershoot between samples, thereby oscillating around a reference value.

8

Experimentally implementing feedback control

We used the control strategy described above to experimentally drive PIF-BFP membrane binding in cells expressing the Phy–PIF module and to drive PHAkt membrane recruitment in cells expressing light-recruitable PI3K activity. For PIF-BFP control, we initially screened cells for their ability to recruit by imaging them after exposure to 30 s of 1V 650 nm light (to measure maximal recruitment) followed by imaging after 30 s of 1V 750 nm light (to observe background fluorescence in the cell lacking recruitment). For PHAkt-Cerulean control, we established cell responsivity by applying 3 minutes of 1V 650 nm light followed by 3 minutes of 1V 750 nm light. We used these maximal and minimal recruitment measurements as guides for picking the range of the target function supplied to our controller.

Because the Phy–PIF system is photoreversible, the voltage range over which 650 nm light drives recruitment can be modulated by simultaneous illumination with a constant level of 750 nm light (**Supplementary Fig. 3a**). For all PIF-BFP control experiments, we applied a feedback-controlled 650 nm light input in combination with a constant 750 nm light input of 0.1 V, so recruitment should vary over a 650 nm input range of 0–0.5 V. In all PI3K control experiments, we applied a constant 750 nm light input of 0.5 V, leading to a tunable 650 nm light range extending from 0–2 V. To experimentally implement PI control of the Phy–PIF interaction, we used the same feedback control algorithm we had applied to our computational model. ON pixels were also always illuminated at a constant level of 750 nm light, and 650 nm LED voltage was set by the PI controller. Recruitment images were acquired once per second, and were automatically processed to return the mean fluorescence intensity in the ON pixel region. Because a PI feedback controller only responds to the error between the measured and desired

9

activity level, subtracting a constant background level has no effect on control; thus, raw intensities were used for all feedback control calculations.

Our computational model predicted that the PI controller could be destabilized by large values of feedback strength or by increasing the time between successive samples. We tested both predictions experimentally by modulating both proportional and integral feedback strength in the range $\phi = 10^{-4}$ to 10^{-1}, and using sampling times of 1 s or 10 s (**Supplementary Fig. 6a,b**). We find that high feedback strength values are destabilizing in either case, but that destabilization happens at a lower strength when recruitment is sampled less frequently. This highlights a general principle of our feedback controller: more frequent sampling permits the use of a broader range of feedback strengths to stably control the cell's response.

Using the feedback controller to decrease cell-to-cell variability in PIF membrane recruitment

We hypothesized that we could tighten the distribution of PIF recruitment levels across a population of cells by using our feedback controller to apply the appropriate light input to each cell. We randomly selected 80 cells expressing Phy-mCherry-CAAX and PIF-BFP, and characterized the expression levels of both optogenetic components (**Supplementary Fig. 7a,b**) as well as the distribution of responses to a uniform, non-saturating light input (0.2 V 650 nm, 0.1 V 750 nm) (**Fig. 2b**). Each cell's fluorescence level in **Fig. 2b** was background-subtracted by measuring the fluorescence in the absence of recruitment. Both Phy–PIF expression levels and PIF membrane recruitment were highly variable between cells. We applied our feedback controller to 60 randomly selected cells from this population, using a reference value set at 60 arbitrary fluorescence units (approximately at the mean of the distribution of PIF recruitment without feedback control), a 1 s sample time, and feedback strengths $\phi_I = \phi_P = 6 \times 10^4$. Using the

controller to tailor the light input delivered to each cell (**Fig. 2c**) led to a tight distribution of PIF

membrane recruitment within 20 s (**Supplementary Fig. 7c**).

3' phosphoinositide production driven by light-recruitable PI3K activity

After developing light-regulated control of PIP_3 generation (**Fig. 3**), we sought to quantify

the spatial range activation of PIP_3 activation, the speed with which PIP_3 activation can be

initiated and terminated, and whether or not cellular signaling feedback connections modulate

PI3K levels in response to prior light-induced activation.

Spatial localization of PI3K recruitment

Membrane recruitment of iSH-YFP-PIF (using an ON pixel mask to illuminate a subset of

the cell) indicated that PIP_3 generation is spatially restricted near the site of PI3K activity

(**Supplementary Fig. 8a**). To quantify this spatial restriction, we measured the decay in PHAkt-

Cerulean signal from the edge of the recruitment region (**Supplementary Fig. 8b**), as well as the

corresponding decay of iSH-YFP-PIF signal (**Supplementary Fig. 8c**). Fitting each of these

profiles to an exponential decay curve (**Supplementary Fig. 8b,c**) revealed that PIP_3 generation

in response to PI3K activation decays by 50% within a spatial range of about 4 μm

(**Supplementary Fig. 8d**), consistent with prior experimental measurements[2, 3]. In contrast, PIF

activation was confined much more closely to the recruitment region, decaying to 50% activity

within 1 μm (**Supplementary Fig. 8d**). Our spatially confined optogenetic PI3K input is a

convenient means to establish the spatial range of PIP_3 in living cells.

Dynamics of PHAkt recruitment

To measure the dynamics of PIP_3 production in response to light-gated PI3K activity, we

measured the increase in PHAkt-Cerulean recruitment in response to activating light (**Fig. 3c;**

Supplementary Fig. 8e,f), and its decrease in response to either inactivating light

11

(**Supplementary Fig. 8e**) or complete inhibition of PI3K activity using LY294002 (**Supplementary Fig. 8f**). We found that recruitment increased to a high level within 200 seconds after stimulation, and that both direct inhibition and light-gated membrane dissociation of PI3K produced similar kinetics of 3' PI lipid disappearance. PI 3-kinase inhibition did not affect the light-gated recruitment of iSH-YFP-PIF, which remained high during LY294002 treatment. We measured the $t_{1/2}$ for 3' PI lipid turnover to be 46 s after exposure to 750 nm light (**Supplementary Fig. 8e**) and 61 s after 100 μM LY294002 treatment (**Supplementary Fig. 8f**), in reasonable agreement with prior measurements for these kinetics (of approximately 35 s)[2]. Our measurements of turnover and spatial decay of 3' PI lipid levels from the site of activation also allow us to estimate the 3' PI lipid diffusion constant, using the equation

$$x_{1/2} = \log(2)\sqrt{\frac{D}{k}} = \log(2)\sqrt{\frac{D \cdot t_{1/2}}{\log(2)}} \ ,$$

providing an estimate for D = 0.50 μm^2 / s, in close agreement with previous estimates (D = 0.35 ± 0.25 μm^2 / s)[2].

Measuring the PI3K-3' PI dose response curve

The light input required to drive a particular membrane concentration of 3' PI lipids depends on the dose response function between light-recruited PI3K and the formation of 3' PI lipids, its enzymatic products. Depending on the regime of enzyme and substrate concentrations and the presence of phosphatases catalyzing the reverse reaction, such a dose response can theoretically range from a graded linear response to a highly ultrasensitive one[4]. We set out to measure the PI3K-3' PI dose response function in individual cells after light stimulation.

One potential complication in performing these measurements arises from the possibility of endogenous feedback regulation of 3' PI lipid levels, known to occur in some cell types (such as

12

leukocytes)[5, 6]. Cellular feedback could cause 3' PI lipids produced by PI3K to depend on the history of prior stimuli applied, making complete dose responses difficult to measure in single cells. To assess whether this issue arises in 3T3 cells, we subjected individual cells to two rounds of PI3K association and dissociation (**Supplementary Fig. 9a**). Neither the kinetics nor total quality of recruitment was changed after two rounds of stimulation, indicating that on a timescale of tens of minutes, no intracellular regulation of 3' PI lipids is engaged (**Supplementary Fig. 9a**). In practice, we observed that maximal recruitment levels remained constant even during individual cell experiments lasting over 30 minutes (data not shown). Thus, to a good approximation, 3' PI lipid dynamics are non-hysteretic in NIH-3T3 fibroblasts.

A second potential challenge in quantifying the relationship between recruited PI3K and 3' PI lipid products can arise if the PHAkt-Cerulean reporter's TIRF signal is not proportional to the membrane concentration of 3' PI lipids. This could arise for two reasons. First, large amounts of 3' PI lipids could deplete the cytoplasmic reservoir of PHAkt-Cerulean, preventing a proportional further increase of its TIRF signal with additional 3' PI lipid production. Second, the observed PHAkt-Cerulean TIRF signal is a weighted combination of both the cytoplasmic and membrane PHAkt levels, so increases in membrane recruitment might be balanced by decrease in the cytoplasmic contribution to fluorescence, making quantitative measurement difficult.

To address this second challenge, we took advantage of the ability to apply spatially restricted light inputs. We restricted PI3K recruitment (and thus 3' PI lipid production) to a small region of membrane, making cytoplasmic PHAkt-Cerulean depletion much less likely than under global cell illumination. Moreover, we were able to quantify any residual cytoplasmic depletion by measuring the PHAkt-Cerulean TIRF signal in light-stimulated cells far from the region of

13

illumination (**Supplementary Fig. 9b**; green curve). If cytoplasmic PHAkt-Cerulean were depleted by recruitment to the illuminated region, the cytoplasmic contribution to TIRF intensity elsewhere in the cell should decrease. This decrease is not observed in our experiments, suggesting that the cytoplasmic level of PHAkt-Cerulean is not limiting.

PHAkt-Cerulean dose response curves were obtained by measuring recruitment at various 650 nm light levels in 10 responsive cells. Measurements of both iSH-YFP-PIF and PHAkt-Cerulean levels were performed after 3 minutes of ON pixel illumination at each of six 650 nm light levels (0, 0.1, 0.2, 0.4, 0.6, and 1V) combined with constant 0.1V 750 nm light (**Supplementary Figs. 9b,c**). Although the recruitment levels in both YFP and Cerulean channels varied between cells, the dose response function between PI3K recruitment and 3' PI lipid product generation was highly linear, with measurements from all 10 cells falling on the same line (**Supplementary Fig. 9d**). This linear result is consistent with previous observations that PI(4,5)P2 substrate levels are high compared to the Michaelis-Menten constant for PI3K modification of this substrate[7]. This analysis demonstrates that the amount of PIP_3 generated in response to a defined amount of membrane-localized PI3K is highly consistent between cells. This observation is notable because the levels of the endogenous p110 PI3K domain and phosphatases such as PTEN and SHIP can vary between cells[8], potentially leading to cell-cell variability in this dose response. Taken together, our results indicate that the PI3K-3' PI step has a linear transfer function and is not hysteretic in 3T3 cells, properties that greatly facilitate our ability to control this signaling molecule with light.

Frequency response of light-gated PI3K activity

To characterize PI3K activity in response to dynamic inputs, we next set out to measure the frequency response of the PI3K module to light. Because 3' PI lipid recruitment is non-hysteretic

14

and roughly proportional to recruited PI3K, we expected that 3' PI levels would oscillate in response to a sinusoidal light input. As in the case of the PIF-BFP frequency response, we applied oscillating light inputs to individual cells at different frequencies. Cells were exposed to each oscillating light input for 5 minutes to allow the system to reach its oscillating steady state. Four periods of light input and PHAkt-Cerulean output data were collected at each frequency and fit to sinusoids, leading to the Bode plots shown in **Supplementary Fig. 4g,h**.

Two effects made measurement of the full PI3K module's frequency response challenging: the low oscillation amplitude of PHAkt-Cerulean membrane binding at high input frequencies, and the length of time that sinusoidal inputs must be applied at low frequencies. Nevertheless, we are able to measure at least one additional pole in the PHAkt response at a lower characteristic frequency than for the PIF-BFP system, indicated by a decrease in frequency at lower amplitude (**Supplementary Fig. 4g**) and the further phase shift of $-\pi/2$ radians from the PIF-BFP response at 0.01 Hz (**Supplementary Fig. 4h**, compare light and dark blue curves). Thus, the frequency response indicates at least one additional first-order transfer function between PIF recruitment and PHAkt binding. These experiments highlight both the strength of applying time-varying inputs to signaling pathways, and the challenges arising from performing measurements of small amplitude signals over long time periods in single cells – challenges which we expect will be overcome by the field in future work.

Limitations and challenges for optogenetic feedback control

Although this work demonstrates robust performance of PI-based optogenetic feedback for a variety of dynamic profiles and activity readouts, there are a number of possible limitations in extending this methodology to arbitrary dynamics and optogenetic inputs. This section is intended to outline some of these considerations for readers interested in extending our methods.

15

First, the feedback controller cannot drive faster dynamics than the response time of the process under control. A practical example of this limitation is that changes in PHAkt-Cerulean levels occur on a timescale of ~45 s (**Fig. 3c,d**), as compared to than changes in PIF-BFP on a timescale of ~5 s (**Fig. 1c**). In addition, the user-defined target function must of course be within the activity range accessible to the controller. For instance, a saturating dose (100 µM) of LY294002 fully inhibits PI3K activity; thus, no amount of feedback-controlled PI3K recruitment would be able to compensate for this effect. Similarly, it is important that serum stimulation (**Fig. 3d**) led to 3' PI lipid levels that did not exceed the set point. This highlights the importance of identifying and optimizing light-activatable signaling inputs with a large dynamic range.

Finally, although a growing number of optogenetic tools are available, the Phy–PIF system stands out as well suited for feedback control of dynamics on a timescale of seconds. The Phy–PIF interaction is reversible and switchable at this timescale (**Supplementary Fig. 2c**). This is a crucial parameter because controlled dynamics are limited by the timescale of the optogenetic input. Second, because the Phy–PIF system is based on protein-protein association, its intracellular activity can be associated with localization change (such as the membrane localization assayed in this work), which is easy to measure in live cells. Direct measurement of activity is necessary for implementing feedback control on the optogenetic input, and to visualize the input level received by the cell.

Although optogenetics is a rapidly changing field and tools are under continuous development, few are currently available with seconds-timescale switching and a direct activity readout in live cells. Nevertheless, some currently available optically-gated techniques might also be especially well-suited for feedback control. For instance, neuronal function can be gated by light-switchable azobenzene derivatives[9] or light control of channelrhodopsin and/or

16

halorhodopsin[10]. Both techniques can be switched quickly, and activation can be measured in live cells by patch clamp or fluorescent sensors of calcium activity. An different approach for feedback control over cell motility than the PI3K system described here might be possible using photoactivatable Rac (PA-Rac) read out by a FRET sensor of Rac activity[11], although the switching time for this system is substantially slower than Phy–PIF ($t_{1/2} \sim 40$ s for the on-off transition, comparable to the turnover rate of PI3K lipid products)[11].

References

[1] J.T. Mettetal, D. Muzzey, C. Gomez-Uribe, A. van Oudenaarden, *Science*, **319**: 482-484 (2008).
[2] I.C. Schneider, J.M. Haugh, *Biophys J*, **86**: 599-608 (2004).
[3] I.C. Schneider, E.M. Parrish, J.M. Haugh, *Biophys J*, **89**: 1420-1430 (2005).
[4] A. Goldbeter, D.E. Koshland, Jr., *Proc Natl Acad Sci U S A*, **78**: 6840-6844 (1981).
[5] O.D. Weiner, P.O. Neilsen, G.D. Prestwich, M.W. Kirschner, L.C. Cantley, H.R. Bourne, *Nat Cell Biol*, **4**: 509-513 (2002).
[6] T. Inoue, T. Meyer, *PLoS ONE*, **3**: e3068 (2008).
[7] I.C. Schneider, J.M. Haugh, *J Cell Biol*, **171**: 883-892 (2005).
[8] T.L. Yuan, G. Wulf, L. Burga, L.C. Cantley, *Curr Biol*, **21**: 173-183 (2011).
[9] M. Banghart, K. Borges, E. Isacoff, D. Trauner, R.H. Kramer, *Nat Neurosci*, **7**: 1381-1386 (2004).
[10] F. Zhang, L.P. Wang, M. Brauner, J.F. Liewald, K. Kay, N. Watzke, P.G. Wood, E. Bamberg, G. Nagel, A. Gottschalk, K. Deisseroth, *Nature*, **446**: 633-639 (2007).
[11] Y.I. Wu, D. Frey, O.I. Lungu, A. Jaehrig, I. Schlichting, B. Kuhlman, K.M. Hahn, *Nature*, **461**: 104-108 (2009).